Met. Mater. Int., Vol. 22, No. 2 (2016), pp. 311~318
doi: 10.1007/s12540-016-5462-6

Non-Vacuum Sintering Process of WC/W2C Reinforced Ni-Based Coating on Steel

Yezhe Lyu[1,2], Yufu Sun[1,*], and Yong Yang[1]

[1]School of Materials Science and Engineering, Zhengzhou University, 97 Wenhua Road, Zhengzhou 450002, PR China
[2]Department of Machine Design, KTH Royal Institute of Technology, SE 100 44 Stockholm, Sweden

(received date: 26 August 2015 / accepted date: 9 December 2015)

Ni-based composite coatings containing varied contents of tungsten carbides on low carbon steel were fabricated. Effects of sintering temperature and tungsten carbides contents on the surface, interface, microstructure and wear resistance of the coatings were investigated using scanning electron microscopy, energy-dispersive X-ray spectroscopy, X-ray diffraction, Vickers microhardness tester, bulk hardness tester and pin-on-disc tribometer. The results indicated that with appropriate sintering temperature (1230 °C), smooth coating surfaces can be achieved. Favorable interfaces about 200 μm can be got that both the chemical composition and property of the interfacial region showed gradual transitions from the substrates to the coatings. Microstructure of the coatings consists of tungsten carbides and M7C3/M23C6 in the matrix. With excessive sintering temperature, tungsten carbides tend to dissolve. Ni-based coatings containing tungsten carbides showed much higher level of bulk hardness and wear resistance than ISO Fe360A and ASTM 1566 steels. With increasing contents of tungsten carbides from 25% to 40%, bulk hardness of Ni-based coatings gradually increased. Ni-based coating with 35% tungsten carbides performed the best wear resistance.

Keywords: coating, sintering, scanning electron microscopy (SEM), X-ray diffraction, wear

1. INTRODUCTION

NiCrBSi based alloys are widely used as coating materials in application areas where the surfaces are subjected to abrasive wear and corrosion [1]. The existence of B and Si in the alloys largely decreases the melting point and endows them with the self-fluxing characteristic [2]. Ni-based alloys are therefore suitable for acting as the binder phase for refractory carbides. By adding appropriate contents of refractory carbides such as TiC, SiC, WC etc., wear resistance of Ni-based coatings can be largely improved [3]. Among these carbides, WC performs a favorable combination of high hardness, wettability and sinterability in the molten binder phase [4-6]. The properties of the Ni-based WC coating, therefore, largely depend on the content, distribution and average size of WC particles, as well as the bonding condition between WC particles and Ni-based matrix [7,8]. In recent years, different surface techniques were applied for producing Ni-based WC coatings [9-14], among which laser cladding is one of the most attractive. However, laser cladding contains some inherent disadvantages because of high thermal stress and self-stirring motion [4]. Cracks are therefore apt to form in the cladding layer [15] and WC is easy to dissolve or sink to the bottom of the coatings [16,17]. Some attempts have been made to overcome the drawbacks of laser cladding technique [3,4,18], the efficiency and controllability, however, are largely declined.

In the recent research project concerning the surface repairing of worn components, an efficient and controllable technique is required to substitute the current laser cladding technique. Referred to literatures [7,19,20], a novel non-vacuum sintering process was utilized to produce Ni-based WC coatings containing tungsten carbides (i.e. WC and W2C) on low carbon steel. Effects of different sintering temperature and content of tungsten carbides were studied around substrate/coating interface, morphology and distribution of tungsten carbides. Besides, bulk hardness and wear resistance of Ni-based WC coatings were discussed compared with conventional carbon steels and laser cladded coatings.

2. EXPERIMENTAL PROCEDURES

2.1. Test specimen preparation

ISO Fe360A mild steel (C ≤ 0.20%, Mn ≤ 1.4%, Si ≤ 0.35%, S ≤ 0.045%, P ≤ 0.045%) was manufactured into rectangular plates (20 mm × 20 mm × 15 mm) and used as the substrate.

*Corresponding author: yufusun@zzu.edu.cn

After cutting, the substrate plates were well treated by grinding and acetone cleaning for eliminating impurities (e.g. engine oil and oxides). Self-fluxing Ni-based alloy powder in size range of 48-74 μm was used as the bonding metal and the chemical composition is shown in Table 1. Cast polycrystalline tungsten carbide powders (mixtures of WC and W2C eutectic) in size range of 60-100 μm were used as the precipitated phase and their scanning electron microscopic (SEM) morphology are shown in Fig. 1. Four different binder contents with 25%, 30%, 35%, and 40% tungsten carbides were designed. After accurate calculation and weighing with analytical balance, appropriate contents of Ni-based alloy and tungsten carbide powders were got and subsequently mixed using a ball milling machine for 12 h. Sodium silicate ($Na_2O{\cdot}3SiO_2$) was applied as the adhesive. The powder mixtures and adhesive were blended into slurries and smeared homogeneously on the substrate to a thickness of 1-2 mm. The substrate with slurries was put into a customized stainless steel die and cold pressed at 100 MPa for 2 min. Before sintering, samples were taken into a two-step drying process (150 °C for 150 min + 400 °C for 10 min) for dislodging the free and crystal water. The coatings were sintered in a temperature-controlled and quasi-sealed furnace at 1200 °C, 1230 °C, 1260 °C for 10 min, respectively. Before sintering, the furnace was vacuumized to 1 Pa and constantly inlet argon for ensuring the inert gas shielding environment. After sintering, samples were cooled in furnace to 400 °C followed by air cooling.

Table 1. Chemical composition (wt%) of Ni-based alloy powders

C	0.3-0.5
Si	3.4-4.5
B	2.5-3.0
Cr	9.0-12.0
Fe	21.0-23.0
Ni	Balance

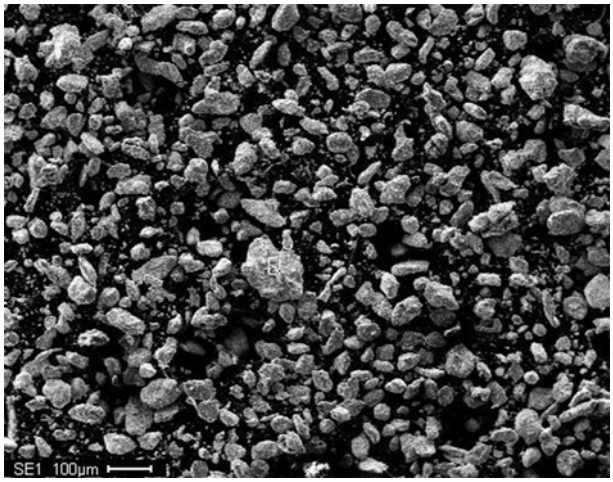

Fig. 1. SEM morphology of tungsten carbides powders.

2.2. Analysis methods

Specimens for metallographic observation, X-ray diffraction (XRD), hardness measurements and wear tests were cut from the sintering samples. Cross-sections of coatings were observed using a Philips-quanta-2000 scanning electron microscopy (SEM) coupled with an energy-dispersive X-ray spectroscopy (EDXS). XRD analysis was conducted on a XPERTPRO-X diffractometer for identifying the phase constitutions and the samples were scanned in 2θ range of 10° to 90°, using Cu-K radiation at 35 kV and 40 mA with a speed of 2° min^{-1}. Vickers type microhardness was measured with a HX-1000TM/LCD tester under 300 g load for 15s. The tests were performed through the cross-sections at various locations for an interval distance of 100 μm. Abrasive wear tests were carried out with a ML-100 pin-on-disc tribometer in room environment (i.e. temperature 20 °C ± 2 °C and relative humidity 40% ± 5%) for evaluating the wear resistance of the coatings with different contents of tungsten carbides. In the wear tests, ISO Fe360A steel used for substrate and ASTM 1566 steel (C: 0.62~0.70%, Si: 0.17~0.37%, Mn: 0.90~1.20%, S ≤ 0.035, P ≤ 0.035) were used as the references. 100# corundum abrasive paper was used as the counterpart material and every test trial was done with a brand new abrasive paper. Specimens in wear test were manufactured into Φ5 × 15 cylinders with a centre-line-average roughness of Ra = 0.6 μm and ultrasonically cleaned with acetone for 2 min before testing. For preventing thermal effects (e.g., local overheating and/or phase transformation), the linear speed was set to 0.1 m s^{-1} and the normal load was 15 N. Each test trial lasted for 35 min, giving a total sliding distance of 210 m. After tests, AB204-N analytical balance with an accuracy of 0.1 mg was used to measure the mass loss. Archard's equation was employed in calculating the wear rate (K_i) of pins [21]:

$$m_i = K_i \cdot F \cdot s \tag{1}$$

where m_i is the mass loss, F the normal force and s the sliding distance. So that the specific wear rate, K_i, could be calculated properly and used to evaluate the wear resistance of different materials. Wear rate is a widely used index to grade the wear resistance and the higher the wear rate the lower the wear resistance of the material [22-24]. Two commercial grades of carbon steel, i.e. ISO Fe360A and ASTM 1566 steels were used as references in the wear tests. Three test trials were conducted for each tungsten carbides content and reference materials to calculate the mean values and standard deviations, which stand for the final grades of wear rate.

3. RESULTS AND DISCUSSION

3.1. Coating surface and interfacial region

The authors observed the coating surface appearances of Ni-based composite coatings containing 35% tungsten car-

bides sintered at 1200 °C, 1230 °C, 1260 °C for 10 min, respectively, and found that the coating sintered at 1230 °C gave the smoothest surface without pores or cracks. While the coating sintered at 1260 °C showed the most rugged surface. A small amount of pores can also be observed on the coating surface sintered at 1200 °C.

Note that there were no cracks being observed on all three surfaces, which can easily be found on the coatings processed by laser cladding [14,15]. The main reason is that laser cladding process often results in the local overheating or high thermal gradients, which may lead to the high residual stresses during solidification and therefore cause cracks [25,26]. The current non-vacuum sintering method slowly and uniformly heated the Ni-based alloy powders and tungsten carbides, getting rid of local overheating or thermal gradients, so that cracks were successfully avoided.

While pores and unevenness were still observed with too low or too high sintering temperature (1200 °C and 1260 °C). One should note that, unlike the local heating during laser cladding process, the mixed Ni-based alloy and tungsten carbides powders were synchronously and uniformly heated during sintering. In addition, an abnormal accumulation of Ni-based alloy was got at the bottom side of substrate plate after sintering at 1260 °C. The observed uneven particles in 1260 °C were therefore considered to be the unmelted tungsten carbide particles. On the contrary, with a too low sintering temperature (1200 °C), the melted Ni-based alloy did not achieve enough flowability to eliminate the air bubbles mixed in the raw slurries and finally left a small amount of pores in the coatings. Meanwhile, ripples which may easily occur from laser cladding and result in unidirectional wear resistance [14,15], were not observed on the non-vacuum sintered surfaces.

Bonding condition between the substrate and coating layer is a significant quality to evaluate the surface coating deposition. An ideal coating should perform a metallurgical bonding with the substrate material and exhibits a thick enough interfacial region [27], which is much thicker and stronger than the laser cladded interface [28,29]. The composition and properties of the interfacial region are supposed to be in between the substrate material and the coating layer, endowing it with sufficient transition and protecting the coating from easy spalling. Figure 2(a) illustrates the cross-section morphologies of Ni-based composite coatings containing 35% tungsten carbides sintered at 1230 °C for 10 min. Obvious interfacial layers can be clearly seen between the substrate and the coating layer, strongly testifying the metallurgical bonding condition

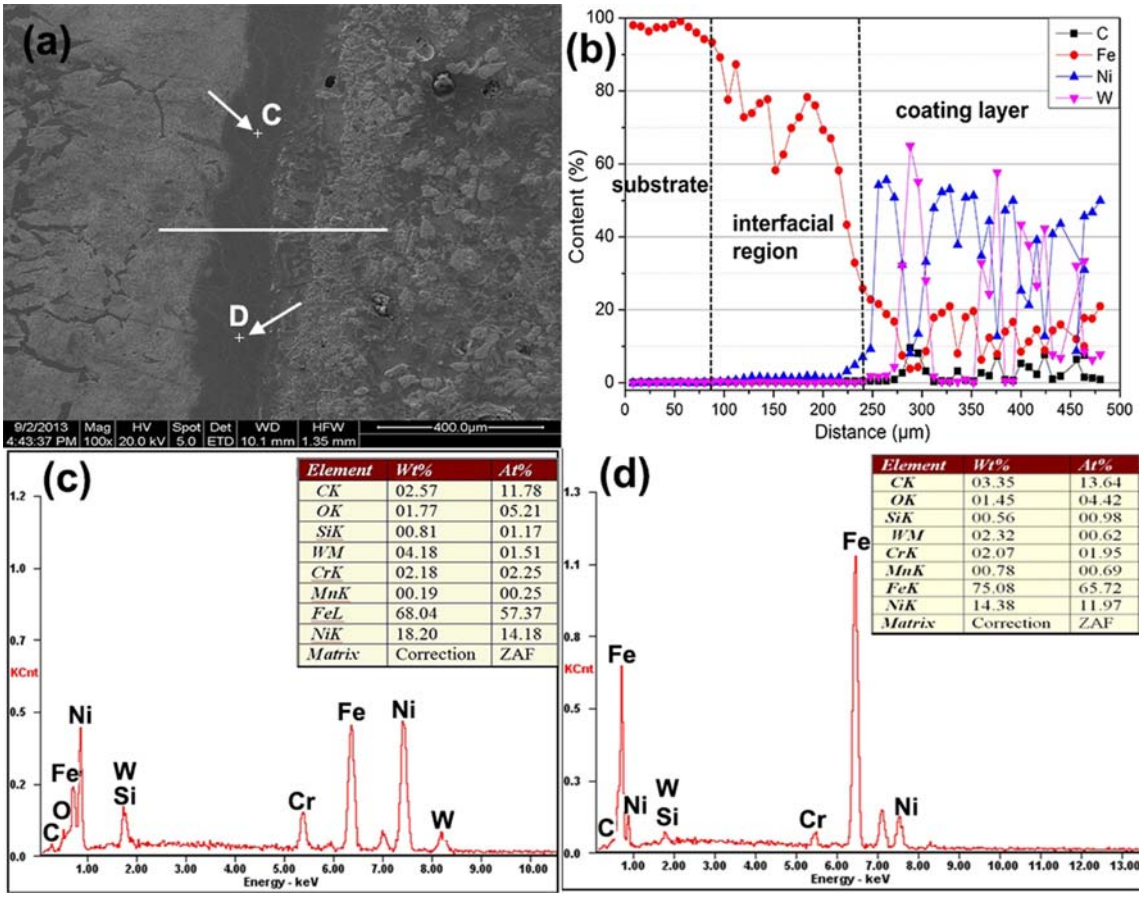

Fig. 2. Cross-section SEM morphology of Ni-based coating containing 35% tungsten carbides sintered at 1230 °C: (a) morphology, (b) line EDS scan result, (c) point EDS scan result of spot C, and (d) point EDS scan result of spot D.

achieved by the non-vacuum sintering method. Meanwhile, with increasing sintering temperature from 1200 to 1260 °C, the average thickness of interfacial layer slightly increased from 176.3 μm to 243.8 μm. (All distances were measured through "Micro-image Analysis & Process" technique). Furthermore, no cracks or pores were observed in the interfacial region, also proving a metallurgical bonding between the substrate and the coating layer [10].

For testing the composition transition of the interfacial layer, one line EDS scan and two point EDS scans were performed on the interfacial layer processed at 1230 °C for 10 min and the results are presented in Fig. 2(b) to 2(d). An apparent and gradual transition of element Fe can be apparently observed in the line EDS scan result (Fig. 2(b)). Element Ni also shows an increase trend from the substrate to the coating layer. Meanwhile, point EDS scan results shown in Figs. 2(c) and 2(d) demonstrate that the concentrations of various elements (e.g. C, Si, Fe and Ni) in the interfacial region lied between the compositions of the substrate material and the coating layer. Therefore, a favorable composition transition got through the non-vacuum sintering method can be declared. Compared with the interface layers (around 2 to 5 μm) from the laser cladding technique [27,30], the interfacial region with current method was much thicker and exhibited an obvious transition of chemical composition from the substrate to the coating layer, guaranteeing the metallurgical bonding.

The microhardness measurements across the transverse cross-section of non-vacuum sintering method can be given to prove the property transition (Fig. 3). The sintering coating layer and substrate are depicted on the right and left hand side, respectively. Interfacial region is highlighted by the perpendicular dotted lines. The microhardness in the coating layers with varied contents of tungsten carbides are between 1200 and 2000 HV, which are slightly beyond the average level of the laser cladding processed coatings [10,13-15]. The extremely high hardness spots (around 2500 HV) might be detected on the hard WC particles. It should be noted that the average levels of microhardness of the samples with 35% and 40% tungsten carbides are obviously higher than the levels of samples containing 25% and 30% tungsten carbides, which is in accordance with several previous researches [28,31,32], demonstrating the reinforcement effect of tungsten carbide particles. Namely, the homogeneous distribution of tungsten carbides and their compacted bonding with Ni-based binder promoted the increase of properties [27]. Furthermore, an intergradation of microhardness in the interfacial region can roughly be observed, which is attributed to the sufficient diffusion of elements shown in Fig. 2 and phase transformation [30]. Favorable transitions of properties as well as chemical compositions in the interfacial region were, therefore, proven to be achieved through the non-vacuum sintering technique, and the interfacial regions showed ideal thicknesses.

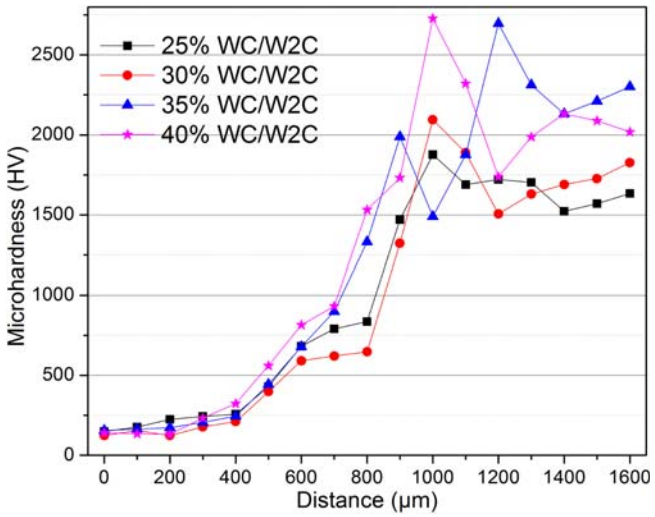

Fig. 3. Microhardness measurements across the cross-section of samples containing different contents of tungsten carbides sintered at 1230 °C for 10 min.

3.2. Microstructural investigation

Figure 4(a) shows the typical microstructure of coating layer, which consists of the matrix and light gray and dark gray phase precipitated in the matrix. For identifying the composition of different phases, point EDS scans were carried out in the same visual field with Fig. 4(a) and the results are presented in Figs. 4(b) to 4(d). From the results, it can be noticed that the light gray phase is almost totally composed of C and W elements (Fig. 4(b)), which can be asserted to be tungsten carbide particles referred to the original morphology shown in Fig. 1. Figure 4(c) illustrates that the matrix was Ni-rich and Fe-rich, which is in accordance to the composition of raw coating powders. The other kind of phase in dark gray color (Fig. 4(d)) performed high concentrations of Cr and C elements, which was suspected to be carbides. The results of XRD analysis presented in Fig. 5 demonstrate the existences of carbides in the forms of M7C3 and M23C6, where M = W, Ni, Cr, Fe and C = C, B. Austerite (i.e. Fe0.64Ni0.36 and Ni2.9Cr0.7Fe0.36) with faced-centered cubic (fcc) crystal, which is the same phase as γ-Ni in references [4,5,13], showed the predominant peaks and formed the matrix of the sintered coating. Besides, WC and W2C occurred in the coating in their original forms from the raw tungsten carbide powders. Note that there are no borides (such as Ni3B or Ni4B3) or other kinds of phases were detected like in other researches of laser cladding [4,5,13,29]. Due to the higher formation temperature of Ni3B than M7C3 and M23C6 carbides [33], the uniform and stable heating through the non-vacuum sintering method can explain the absence of Ni3B or Ni4B3 borides. A more homogenous microstructure can be, therefore, ensured with lower lattice deformation and stress concentration.

The general distribution of tungsten carbides in the coating

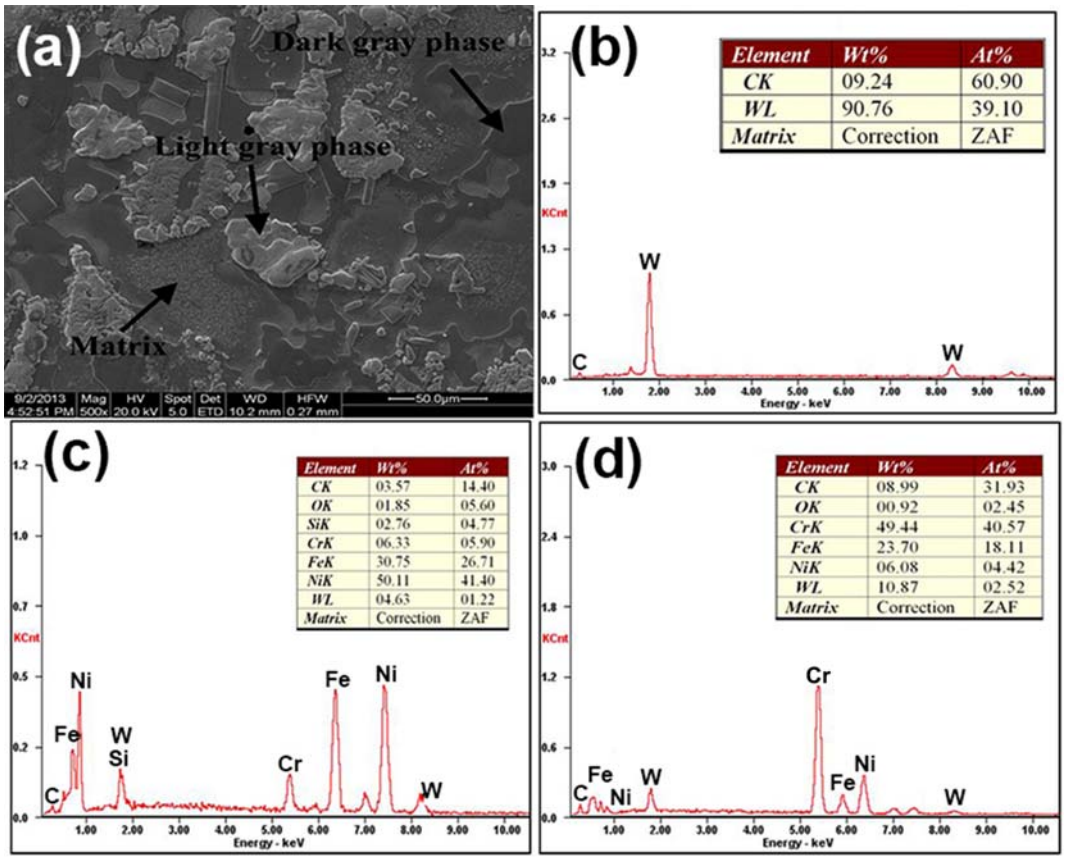

Fig. 4. (a): Typical SEM microstructure of the coating layer containing 35% tungsten carbides sintered at 1230 °C for 10 min and EDS scan results of (b) light gray phase, (c) matrix, and (d) dark gray phase shown in Fig. 4a.

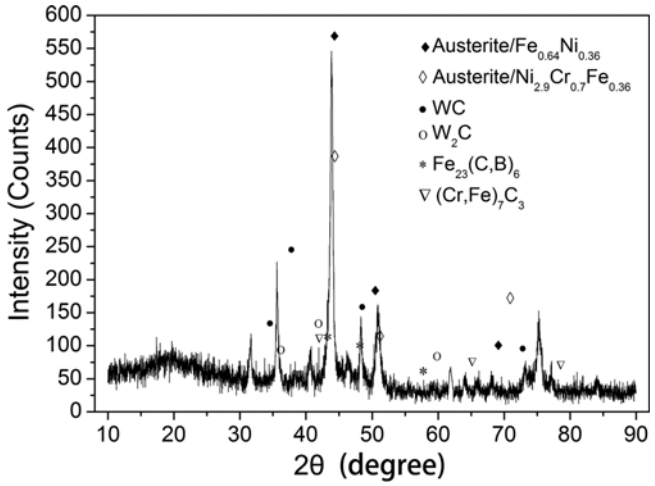

Fig. 5. Result of XRD analysis of the coating containing 35% tungsten carbides sintered at 1230 °C for 10 min.

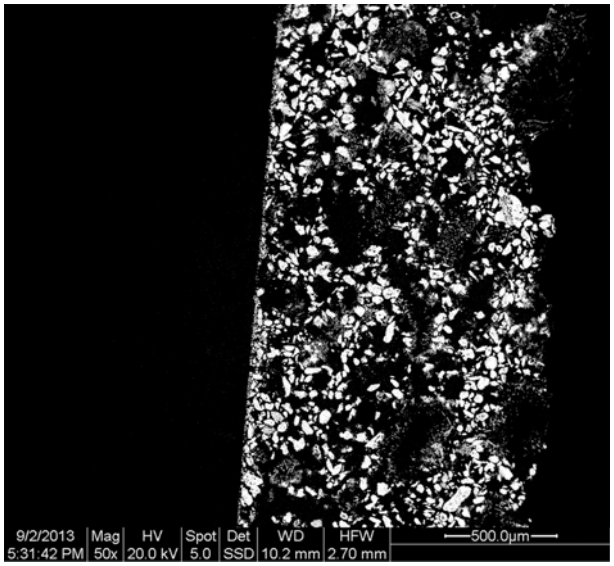

Fig. 6. General distribution of tungsten carbides in the coating (left dark part is the substrate and interfacial region).

was also observed through BSE technique which is shown Fig. 6. It can be noticed that the bright WC particles distributed homogenously in the coating layer. The extremely common sinkage and accumulation of WC to the substrate boundary through laser cladding is not found with the current non-vacuum sintering method [14,34]. The main reason is that there was no stirring within the sintering method, unlike the laser cladding technique with self-stirring, so that the surface ten-

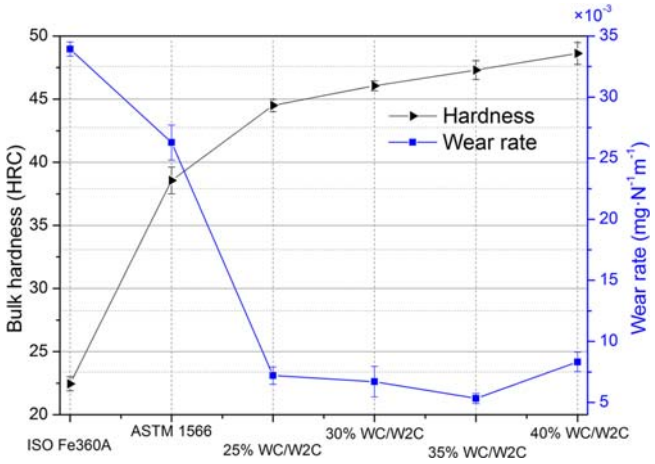

Fig. 7. Bulk hardness and wear rate of Ni-based composite coatings as a function of tungsten carbide contents. ISO Fe360A substrate and ASTM 1566 steel are applied as reference.

sion and the sodium silicate adhesive can effectively hold the tungsten carbide powders in the Ni-based alloy slurries, although the density of WC is much higher than the Ni-based alloy. Therefore, more uniform properties and performance of the sintered coating can be expected through this non-vacuum sintering method.

3.3. Bulk hardness and wear resistance

Figure 7 shows the bulk hardness and wear rate of Ni-based composite coatings as a function of tungsten carbides contents. ISO Fe360A and ASTM 1566 steels are presented as references. Wear rate is the most common feature for evaluating the wear resistance of materials and a low level of wear rate is corresponding to a favorable wear resistance. It is obvious that the bulk hardness largely increased with the existence of Ni-based coatings compared with ISO Fe360A substrate and ASTM 1566 steel. Meanwhile, wear rates of samples containing composite coatings decreased dramatically compared with coating-free samples (i.e. ISO Fe360A and ASTM 1566 steels). Also note that, among the coating samples, bulk hardness experienced a gradual increase with the increasing tungsten carbide contents from 25% to 40% while wear rates first

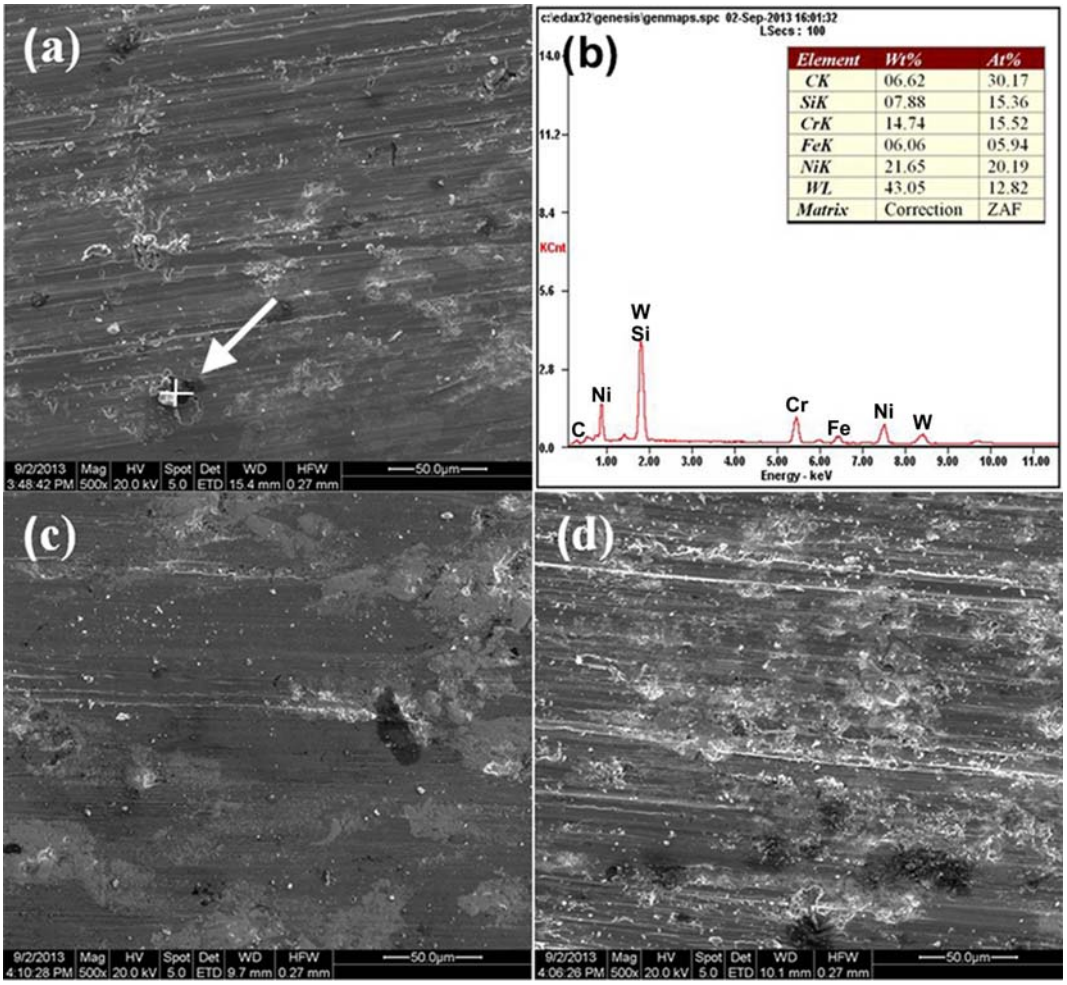

Fig. 8. Worn surfaces of Ni-based coatings containing (a) 25% tungsten carbides, (b) point EDXS analysis marked by arrow, (c) 35% tungsten carbides, and (d) 40% tungsten carbides.

decreased and then increased. This phenomena is similar with several previous studies [1,6,14], which show that excessive WC may destroy the wear resistance of the Ni-based coatings.

Bulk hardness is a comprehensive property of material's ductility, elasticity, strength etc., which performs as the ability to resist permanent deformation against compressive force. Dispersed phase will evidently influence the hardness together with the matrix [35]. In the current research, the increasing content and well-dispersion of tungsten carbides effectively reinforced the matrix and resisted the local deformation, leading to the increment of bulk hardness. The sharp decrease of wear rate of samples with deposition of Ni-based WC/W2C coatings, compared with coating-free ISO Fe360A and ASTM 1566 steels, is mainly ascribed to the much higher level of bulk hardness [36]. While with the increasing content of tungsten carbides, the first decrease and subsequent increase of wear rate can hardly be explained. Here, it should also be noted that when precipitated particles were applied, their interaction with matrix usually acts an important role in preventing the materials from wear [37-39]. Under such circumstance, the common belief that a higher hardness gives a higher wear resistance becomes not always reliable [36]. Therefore, analyzing the wear mechanisms of samples containing varied contents of tungsten carbides is necessary to explain the phenomenon of wear rate alterations.

During the abrasive wear process, wear loss may happen through three major forms: (1) micro-cutting, (2) plastic deformation and (3) spalling of hard-phase debris, among which the spalling is popularly believed to be the greatest contribution to the wear loss [1]. Figure 8 presents the worn surfaces of Ni-based coatings containing different contents of tungsten carbides. It can be seen from Fig. 8a that large scale of plastic deformation parallel to sliding direction occupied the worn surface together with small amount of white tiny wear debris. Hard particles embedded the coatings can also be observed (marked by arrow). The corresponding EDXS result shown in Fig. 8b clearly identified it to be a tungsten carbide particle. With the tungsten carbides increased to 35%, some tiny wear debris can also be observed on the worn surface shown in Fig. 8c. While the quantity of wear debris, compared with samples containing 25% tungsten carbides, is apparently less. Besides, polishing-like micro-cutting features largely occupied the surface instead of plastic deformation, demonstrating a milder wear condition. Differently, a large amount of wear debris can be observed in Fig. 8d, which may be sheared off during wear process and observed in previous studies [10,12,18,40]. These countless sheared off hard particles will participate the wear process as third-bodies and promote the wear loss, resulting in the highest wear rate of 40% tungsten carbides sintered coating, compared with other sintered coatings. This is in accordance to several researches that with large amount of wear debris, the abrasive wear was accelerated [36,40].

4. CONCLUSIONS

(1) Sintering temperature influenced the surface appearance of sintered coatings. With appropriate sintering temperature (1230 °C), smooth coating surfaces without cracks and pores can be achieved within argon shielding environment.

(2) Favorable interfacial regions about 200 μm can be got with different sintering temperature and both the chemical composition and property of the interfacial region showed gradual transitions from the substrates to the coatings.

(3) Microstructure of the coating layers consists of tungsten carbides and M7C3/M23C6 carbides in a matrix of austenite. Borides which damage the homogeneity of microstructure were not found.

(4) Tungsten carbides uniformly distributed in the coating layers. With excessive sintering temperature, tungsten carbides tend to dissolve and be diluted by the matrix.

(5) Ni-based coatings containing tungsten carbides showed much higher level of bulk hardness and wear resistance compared with ISO Fe360A and ASTM 1566 steels. With increasing tungsten carbide contents from 25% to 40%, bulk hardness of Ni-based coatings gradually increased while wear rate firstly decrease and then increased. Ni-based coating with 35% tungsten carbides performed the lowest wear rate.

REFERENCES

1. H. Wang, W. M. Xia, and Y. S. Jin, *Wear* **195**, 47 (1996).
2. M. J. Tobar, C. Álvarez, J. M. Amado, G. Rodríguez, and A. Yáñez, *Surf. Coat. Tech.* **200**, 6313 (2006).
3. S. Zhou, Y. Huang, and X. Zeng, *Appl. Surf. Sci.* **254**, 3110 (2008).
4. S. Zhou, Y. Huang, X. Zeng, and Q. Hu, *Mater. Sci. Eng. A* **480**, 564 (2008).
5. S. Zhou, X. Zeng, Q. Hu, and Y. Huang, *Appl. Surf. Sci.* **255**, 1646 (2008).
6. J. Qu, W. Xiong, D. Ye, Z. Yao, W. Liu, and S. Lin, *Int. J. Refract. Met. H.* **28**, 243 (2010).
7. E. Taheri-Nassaj and S. H. Mirhosseini, *J. Mater. Process. Tech.* **142**, 422 (2003).
8. L. Y. Sheng, F. Yang, T. F. Xi, and J. T. Guo, *J. Alloy. Compd.* **554**, 182 (2013).
9. L.-M. Berger, *Int. J. Refract. Met. H.* **49**, 350 (2015).
10. S. Chen, J. Liang, C. Liu, K. Sun, and J. Mazumder, *Appl. Surf. Sci.* **258**, 1443 (2011).
11. Y. Lyu, Y. Sun, and F. Jing, *Ceram. Int.* **41**, 10934 (2015).
12. N. Serres, F. Hlawka, S. Costil, C. Langlade, and F. Machi, *Appl. Surf. Sci.* **257**, 5132 (2011).
13. P. Wu, H. M. Du, X. L. Chen, Z. Q. Li, H. L. Bai, and E. Y. Jiang, *Wear* **257**, 142 (2004).
14. C. Guo, J. Chen, J. Zhou, J. Zhao, L. Wang, Y. Yu, and H. Zhou, *Surf. Coat. Tech.* **206**, 2064 (2012).
15. C. P. Paul, H. Alemohammad, E. Toyserkani, A. Khajepour, and S. Corbin, *Mater. Sci. Eng. A* **464**, 170 (2007).

16. G. Y. Liang and T. T. Wong, *J. Mater. Eng. Perform.* **6**, 41 (1997).
17. P. H. Chong, H. C. Man, and T. M. Yue, *Surf. Coat. Tech.* **145**, 51 (2001).
18. F. Luo, A. Cockburn, M. Sparkes, R. Lupoi, Z.-J. Chen, W. O'Neill, J.-H. Yao, and R. Liu, *Defence Technology* **11**, 35 (2015).
19. Y. L. Yan, Y. Zheng, H. J. Yu, H. J. Bu, X. Cheng, and N. W. Zhao, *Powder. Metall. Met. C*+ **46**, 449 (2007).
20. E. O. Correa, J. N. Santos, and A. N. Klein, *Int. J. Refract. Met. H.* **28**, 572 (2010).
21. J. Archard and W. Hirst, *P. Roy. Soc. Lond. A. Mat.* **236**, 397 (1956).
22. Y. Lyu, E. Bergseth, U. Olofsson, A. Lindgren, and M. Höjer, *Wear* **338-339**, 36 (2015).
23. Y. Lyu, Y. Zhu, and U. Olofsson, *Wear* **328-329**, 277 (2015).
24. Y. Zhu, Y. Lyu, and U. Olofsson, *Wear* **324-325**, 122 (2015).
25. U. de Oliveira, V. Ocelík, and J. T. M. De Hosson, *Surf. Coat. Tech.* **201**, 533 (2006).
26. U. de Oliveira, V. Ocelík, and J. T. M. De Hosson, *Surf. Coat. Tech.* **201**, 6363 (2007).
27. Q.-Y. Wang, S.-L. Bai, Y.-F. Zhang, and Z.-D. Liu, *Appl. Surf. Sci.* **308**, 285 (2014).
28. C. Cui, F. Ye, and G. Song, *Surf. Coat. Tech.* **206**, 2388 (2012).
29. Q. Li, T. C. Lei, and W. Z. Chen, *Surf. Coat. Tech.* **114**, 285 (1999).
30. X.-M. He, X.-B. Liu, M.-D. Wang, M.-S. Yang, S.-H. Shi, G.-Y. Fu, and S.-F. Chen, *Appl. Surf. Sci.* **258**, 535 (2011).
31. J. Iwaszko, *Surf. Coat. Tech.* **201**, 3443 (2006).
32. H.-F. Xuan, Q.-Y. Wang, S.-L. Bai, Z.-D. Liu, H.-G. Sun, and P.-C. Yan, *Surf. Coat. Tech.* **244**, 203 (2014).
33. C. B. Finch, O. B. Cavin, and P. F. Becher, *J. Cryst. Growth.* **67**, 556 (1984).
34. H. Liu, C. Wang, X. Zhang, Y. Jiang, C. Cai, and S. Tang, *Surf. Coat. Tech.* **228**, 296 (2013).
35. Y. Sun, Y. Lyu, A. Jiang, and J. Zhao, *J. Mater. Res.* **29**, 260 (2014).
36. G. Hu, H. Meng, and J. Liu, *Appl. Surf. Sci* **317**, 378 (2014).
37. Y. Lv, Y. Sun, J. Zhao, G. Yu, J. Shen, and S. Hu, *Mater. Design* **39**, 303 (2012).
38. Y. Sun, Y. Lv, L. Wang, J. Shen, X. Jia, and J. Zhao, *Oxid. Met.* **80**, 113 (2012).
39. Y. F. Sun, Y. Z. Lv, Y. Zhang, J. Y. Zhao, and Y. Wu, *Mater. Sci. Tech. Ser.* **29**, 511 (2013).
40. S. F. Gnyusov and S. Y. Tarasov, *Appl. Surf. Sci.* **293**, 318 (2014).